

A Galerkin-Collocation domain decomposition method: application to the evolution of cylindrical gravitational waves

W O Barreto^{1,2}, J A Crespo², H P de Oliveira² and E L Rodrigues³

¹ Centro de Física Fundamental, Universidad de Los Andes, Mérida 5101, Venezuela

² Departamento de Física Teórica - Instituto de Física A. D. Tavares, Universidade do Estado do Rio de Janeiro, R. São Francisco Xavier, 524. Rio de Janeiro, RJ, 20550-013, Brazil

³ Instituto de Biociências - Departamento de Física, Universidade Federal do Estado do Rio de Janeiro, Av. Pasteur, 458 - Urca. Rio de Janeiro, RJ, 22290-040, Brazil

Abstract. We present a Galerkin-Collocation domain decomposition algorithm applied to the evolution of cylindrical unpolarized gravitational waves. We show the effectiveness of the algorithm in reproducing initial data with high localized gradients and in providing highly accurate dynamics. We characterize the gravitational radiation with the standard Newman-Penrose Weyl scalar Ψ_4 . In the sequence, it was possible to generate wave templates in situations of interest, in particular, those corresponding to the interaction of both gravitational wave modes at the radiation zone.

Keywords: Numerical Relativity, Galerkin-Collocation, Cylindrical Gravitational Waves.
Submitted to: *Class. Quantum Grav.*

1. Introduction

In the last years, we have witnessed the growing popularity of spectral methods in numerical relativity with applications in a large variety of problems [1]. The main advantage of spectral methods when compared with the traditional finite difference methods is the superior accuracy for a fixed number of grid points [2]. In particular, for smooth functions, the convergence rate exhibited by spectral methods is exponential. On the other hand, the accuracy of spectral methods in solving partial differential equations is drastically reduced in the case the solutions have localized regions of rapid variations, or if the spatial domain has a complex geometry [3, 4].

Multidomain techniques [3, 5, 6, 7, 8] or simply the domain decomposition method is a beautiful and efficient strategy to improve the accuracy of spectral approximations for the cases mentioned above. The spatial domain is divided into two or more subdomains, where we can establish spectral approximations of a function in each subdomain together with the matching or transmissions conditions across the subdomains boundaries. In this work, we have the set up a version of the spectral fixed mesh refinement.

In numerical relativity, the first applications of the domain decomposition technique involved the determination of the stationary configurations [9] and the initial data problem [10, 11], mainly for binaries of black holes. For the time-dependent systems, the spectral domain decomposition was implemented within the SpEC [12] and LORENE [13] codes to deal with the gravitational collapse, the dynamics of stars and the evolution of single [14] and binary black holes [15].

We point out that a crucial step for the implementation the domain decomposition technique is the treatment of the transmission conditions in the cases of non-overlapping and overlapping subdomains. Let us consider, for instance, non-overlapping subdomains. For the time-independent situations such as the initial data problem described by elliptic equations, it is necessary to guarantee the smoothness of a function and its normal derivative on the surface the subdomains touch. On the other hand, hyperbolic problems require, in general, different interface conditions than elliptic ones known as the upwind, downwind and average scheme [6, 3, 16]. Mainly, these schemes comprise the way in which the weights of the contributions from the subdomains to update the equation at the common interface.

The aim of the present work is twofold. First, we present an innovative Galerkin-Collocation domain decomposition algorithm to evolve general cylindrical gravitational waves. We have divided the physical spatial domain into two subdomains and introduced the corresponding computational subdomains which are the loci of the collocation points. The communication between the physical and the computational subdomains is established by distinct mappings that cover the whole spatial domain. Second, we explore the consequences of the interaction between the gravitational wave polarization modes by generating the wave templates associated with the polarization modes at the radiation zone. Although cylindrical gravitational waves do not represent a real physical situation, they provide a useful theoretical laboratory to investigate the interaction of the polarization wave modes [17].

We organized the paper as follows. In Section II, we present the basic equations of the general cylindrical gravitational waves. The Galerkin-Collocation domain decomposition method is described in details in Section III, along with the numerical scheme to evolve the field equations. Section IV deals with the validation of the code through numerical tests of convergence. We have discussed the physical aspects in Section V by establishing the version of the peeling theorem for cylindrical spacetimes. In the sequence, we obtain the expression for the Weyl scalar, Ψ_4 , that determines the templates of the gravitational waves at the wave zone, with a special interest in those resulting from the interaction between both polarization modes. We close this work with some final remarks in Section 6.

2. Basic equations

We have considered the general cylindrical line element originally proposed by Kompaneets [18] and Jordan *et al.* [19] in null coordinates,

$$ds^2 = -e^{2(\gamma-\psi)}(du^2 + 2 du d\rho) + e^{2\psi}(dz + \omega d\phi)^2 + \rho^2 e^{-2\psi} d\phi^2, \quad (1)$$

where u is the retarded null coordinate that foliates the spacetime in hypersurfaces $u = \text{constant}$ and (ρ, z, ϕ) are the usual cylindrical coordinates. The metric functions ψ , ω , γ depend on u and ρ . As a well-known important aspect of cylindrical spacetimes [20], the functions ψ and ω represent the two dynamical degrees of freedom of the gravitational field, in which ψ accounts for the polarization mode $+$ while ω the polarization mode \times [20]. The function γ plays the role of the gravitational energy of the system; it is connected to the C-energy [20, 21, 22], more precisely $\gamma(\rho, u)$ gives the total energy per unit length enclosed within a cylinder of radius ρ at the time u .

Following Refs. [23, 24] it is convenient to introduce a new radial coordinate y by

$$\rho = y^2, \quad (2)$$

and to define the new fields $\bar{\psi}$ and $\bar{\omega}$, respectively by

$$\bar{\psi} = y\psi, \quad (3)$$

$$\bar{\omega} = \frac{\omega}{y}. \quad (4)$$

Thus, the field equations in terms of the new fields $\bar{\psi}$ and $\bar{\omega}$ are expressed by

$$y\bar{\psi}_{,uy} - \frac{e^{4\bar{\psi}/y}}{2y}(y\bar{\omega})_{,y}\bar{\omega}_{,u} - \frac{1}{4} \left[y \left(\frac{\bar{\psi}}{y} \right)_{,y} \right]_{,y} + \frac{e^{4\bar{\psi}/y}}{8y^3}(y\bar{\omega})_{,y}^2 = 0, \quad (5)$$

$$y\bar{\omega}_{,uy} + \frac{2}{y}(y\bar{\omega})_{,y}\bar{\psi}_{,u} + 2y \left(\frac{\bar{\psi}}{y} \right)_{,y} \bar{\omega}_{,u} - \frac{y^2}{4} \left[\frac{(y\bar{\omega})_{,y}}{y^3} \right]_{,y} - \frac{1}{y}(y\bar{\omega})_{,y} \left(\frac{\bar{\psi}}{y} \right)_{,y} = 0, \quad (6)$$

where the subscripts u and y denote partial derivatives with respect to these coordinates.

The dynamics of cylindrical spacetimes is fully described by the coupled wave equations (5) and (6) for the gravitational potentials $\bar{\psi}, \bar{\omega}$ starting with the initial data functions $\bar{\psi}_0(y) = \bar{\psi}(u_0, y)$ and $\bar{\omega}_0(y) = \bar{\omega}(u_0, y)$. These initial distributions are free of any constraint according with the characteristic scheme we adopt here.

The metric function γ satisfies the remaining field equations

$$\gamma_{,y} = \frac{y}{2} \left(\frac{\bar{\psi}}{y} \right)_{,y}^2 + \frac{e^{4\bar{\psi}/y}}{8y^3} (y\bar{\omega})_{,y}^2, \quad (7)$$

$$\gamma_{,u} = \bar{\psi}_{,u} \left(\frac{\bar{\psi}}{y} \right)_{,y} - 2\bar{\psi}_{,u}^2 + \frac{e^{4\bar{\psi}/y}}{4y^2} [\bar{\omega}_{,u} (y\bar{\omega})_{,y} - 2y^2 \bar{\omega}_{,u}^2]. \quad (8)$$

Thus, the evolution of $\gamma(u, y)$ is determined after solving the wave equations (5) and (6).

The boundary conditions embody the well behaved coordinates as well as the regularity for the spacetime. After a careful inspection of the field equations (5) and (6), the conditions of regularity and flatness of the metric near the origin $y = 0$ impose that

$$\bar{\psi}(u, y) = \mathcal{O}(y), \quad (9)$$

$$\bar{\omega}(u, y) = \mathcal{O}(y^3). \quad (10)$$

The other boundary conditions are specified at the outer boundary or at the future null infinity, \mathcal{I}^+ ($y = \infty$). The asymptotic analysis [21] of the wave equations (5) and (6) leads to

$$\bar{\psi}(u, y) = \bar{\psi}_\infty(u) + \mathcal{O}(y^{-1}), \quad (11)$$

$$\bar{\omega}(u, y) = \bar{\omega}_\infty(u) + \mathcal{O}(y^{-2}), \quad (12)$$

where $\bar{\psi}_\infty(u)$ and $\bar{\omega}_\infty(u)$ are arbitrary functions. Then, the spacetime is not asymptotically flat.

3. The Galerkin-Collocation domain decomposition method

We present here the domain decomposition algorithm for the dynamics of general cylindrical gravitational waves. In Ref. [24] we have implemented a single domain method for the same problem. However, we have made a comment about the lack of exponential convergence using the single domain code to testing it against the Xanthopoulos exact solution [25] that contains both gravitational degrees of freedom $\bar{\psi}$ and $\bar{\omega}$. In general, the exact profiles exhibit rapid variations of the corresponding fields that spoil the exponential convergence for the case of one domain code. A domain decomposition algorithm improves the convergence as we indicated briefly in [24]. In what follows, we present the details.

We begin by dividing the spatial domain in two subdomains: $\mathcal{D}_1 : 0 \leq y \leq y_0$ and $\mathcal{D}_2 : y_0 \leq y < \infty$, where $y = y_0$ is the interface between both domains. The equivalent

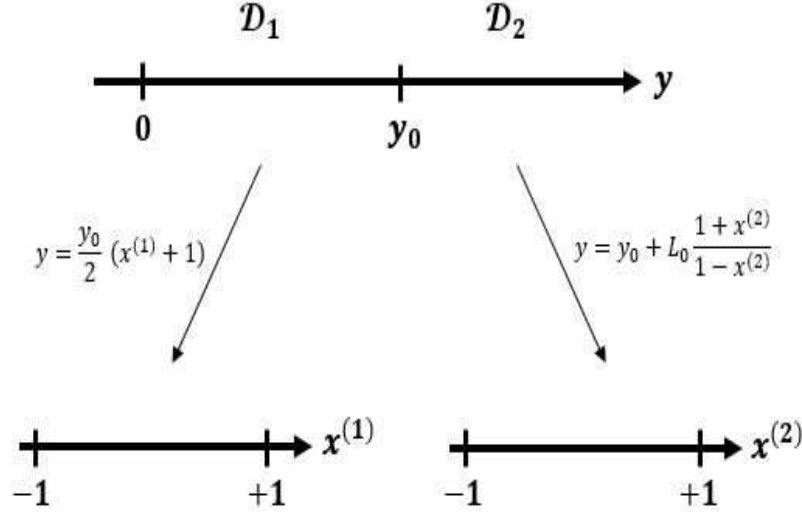


Figure 1. Basic scheme showing the subdomains $\mathcal{D}_1 : 0 \leq y \leq y_0$ and $\mathcal{D}_2 : y_0 \leq y < \infty$ and the corresponding maps to the computational variable $x^{(A)}$ where $-1 \leq x^{(A)} \leq 1$ with $A = 1, 2$.

computational subdomains are indicated by $\mathcal{D}_A : -1 \leq x^{(A)} \leq 1$, with $A = 1, 2$ (cf. Fig. 1). We have chosen the following maps that connect the computational and physical subdomains:

$$\mathcal{D}_1 : y = \frac{y_0}{2}(1 + x^{(1)}), \quad (13)$$

$$\mathcal{D}_2 : y = y_0 + L_0 \frac{(1 + x^{(2)})}{(1 - x^{(2)})}, \quad (14)$$

where L_0 is the map parameter.

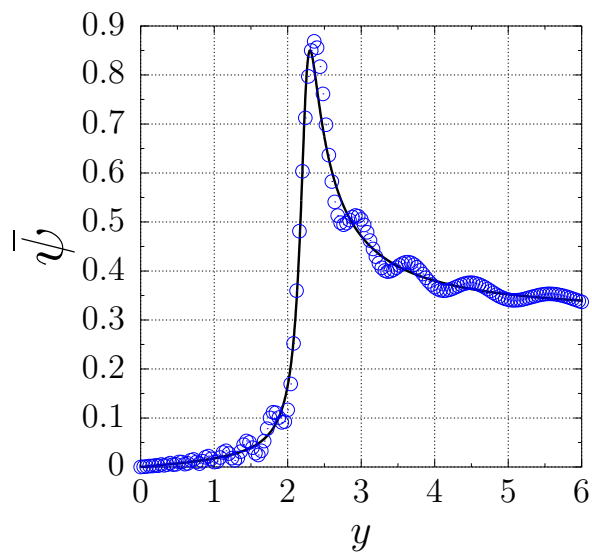
In each subdomain \mathcal{D}_A , $A = 1, 2$, we establish the spectral approximations for the gravitational potentials $\bar{\psi}$ and $\bar{\omega}$ as

$$\bar{\psi}^{(A)}(u, y) = \sum_{k=0}^{N_{\bar{\psi}}^{(A)}} a_k^{(A)}(u) \Psi_k^{(A)}(y), \quad (15)$$

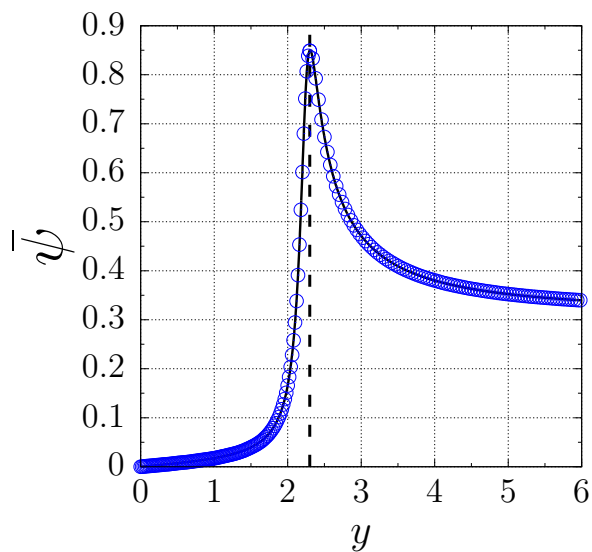
$$\bar{\omega}^{(A)}(u, y) = \sum_{k=0}^{N_{\bar{\omega}}^{(A)}} b_k^{(A)}(u) \Phi_k^{(A)}(y), \quad (16)$$

where $N_{\bar{\psi}}^{(A)}$ and $N_{\bar{\omega}}^{(A)}$ are the truncations orders, not necessarily equal, that dictate the number of unknown modes $a_j^{(A)}(u)$ and $b_k^{(A)}(u)$, respectively. According to the Galerkin method, the basis functions $\Psi_j^{(A)}(y)$ and $\Phi_k^{(A)}(y)$ satisfy the boundary conditions (9) - (12) by combining conveniently the rational Chebyshev polynomials defined in each subdomain. The rational Chebyshev polynomials [26] defined in each subdomain are

$$TL_k^{(1)}(y) = T_k \left(x^{(1)} = \frac{2y}{y_0} - 1 \right), \quad (17)$$



(a)



(b)

Figure 2. Exact initial profile provided by the Weber-Wheeler solution (see Eq. B1) with $A_0 = 1.0$, $a = 2$ and $u_0 = -10$. In both graphs, the continuous lines and the circles correspond to the exact and the numerical solutions, respectively. It becomes clear that the numerical solution generated by the single domain algorithm with $N_\psi = 60$ (panel (a)) is less accurate than the one obtained with the domain decomposition algorithm with $N_\psi^{(1)} = N_\psi^{(2)} = 20$ (panel (b)). Here we assumed that $y_0 = L_0 = 2.3$.

$$TL_k^{(2)}(y) = T_k \left(x^{(2)} = \frac{y - y_0 - L_0}{y - y_0 + L_0} \right). \quad (18)$$

where $T_k(x)$ represents the standard Chebyshev polynomial of k th-order. We present below the basis functions:

$$\begin{aligned} \Psi_k^{(1)}(y) &= \frac{1}{2}(TL_{k+1}^{(1)}(y) + TL_k^{(1)}(y)), \\ \Psi_k^{(2)}(y) &= TL_k^{(2)}(y), \\ \Phi_k^{(2)}(y) &= \Psi_k^{(2)}(y), \end{aligned} \quad (19)$$

and the corresponding expression to $\Phi_k^{(1)}(y)$ can be found in the Appendix A.

We have followed the domain decomposition method straightforwardly for hyperbolic problems according to Gottlieb and Orszag [5]. In their approach, the junction or transmission conditions are

$$\begin{aligned} \bar{\psi}^{(1)}(u, y_0) &= \bar{\psi}^{(2)}(u, y_0), \\ \left(\frac{\partial \bar{\psi}^{(1)}}{\partial y} \right)_{y_0} &= \left(\frac{\partial \bar{\psi}^{(2)}}{\partial y} \right)_{y_0}, \\ \bar{\omega}^{(1)}(u, y_0) &= \bar{\omega}^{(2)}(u, y_0), \\ \left(\frac{\partial \bar{\omega}^{(1)}}{\partial y} \right)_{y_0} &= \left(\frac{\partial \bar{\omega}^{(2)}}{\partial y} \right)_{y_0}. \end{aligned} \quad (20)$$

Taking into account the spectral approximations of the metric functions (15) and (16) into the above transmission conditions, we obtain four linear equations involving the coefficients $a_k^{(A)}(u)$ and $b_k^{(A)}(u)$, $A = 1, 2$. Furthermore, these relations are used to reduce the total number of independent coefficients of $\bar{\psi}^{(A)}$ and $\bar{\omega}^{(A)}$ to $N_\psi^{(1)} + N_\psi^{(2)} + 2 - 2 = N_\psi^{(1)} + N_\psi^{(2)}$ and $N_\omega^{(1)} + N_\omega^{(2)} + 2 - 2 = N_\omega^{(1)} + N_\omega^{(2)}$, respectively.

We proceed by establishing the residual equations by substituting the approximations (15) and (16) into the field equations (5) and (6) which yields

$$\begin{aligned} \text{Res}_\psi^{(A)}(u, y) &= y\bar{\psi}_{,uy}^{(A)} - \frac{e^{4\bar{\psi}^{(A)}/y}}{2y}(y\bar{\omega}^{(A)})_{,y}\bar{\omega}_{,u}^{(A)} - \frac{1}{4} \left[y \left(\frac{\bar{\psi}^{(A)}}{y} \right)_{,y} \right]_{,y} \\ &\quad + \frac{e^{4\bar{\psi}^{(A)}/y}}{8y^3}(y\bar{\omega}^{(A)})_{,y}^2, \end{aligned} \quad (21)$$

$$\begin{aligned} \text{Res}_\omega^{(A)}(u, y) &= y\bar{\omega}_{,uy}^{(A)} + \frac{2}{y}(y\bar{\omega}^{(A)})_{,y}\bar{\psi}_{,u}^{(A)} + 2y \left(\frac{\bar{\psi}^{(A)}}{y} \right)_{,y} \bar{\omega}_{,u}^{(A)} - \frac{y^2}{4} \left[\frac{(y\bar{\omega}^{(A)})_{,y}}{y^3} \right]_{,y} \\ &\quad - \frac{1}{y}(y\bar{\omega}^{(A)})_{,y} \left(\frac{\bar{\psi}^{(A)}}{y} \right)_{,y}. \end{aligned} \quad (22)$$

In general the residuals $\text{Res}_\psi^{(A)}(u, y)$ and $\text{Res}_\omega^{(A)}(u, y)$ do not vanish since $\bar{\psi}^{(A)}$ and $\bar{\omega}^{(A)}$ are approximations to the exact corresponding gravitational potentials. In according with the

numerical strategy we are adopting, we use the Collocation method in the sense that the residual equations vanish at the collocation or grid points. Schematically we may write

$$\text{Res}_\psi^{(A)}(u, y_k) = 0, \quad k = 0, 1, \dots, N_\psi^{(A)} - 1, \quad (23)$$

$$\text{Res}_\omega^{(A)}(u, y_k) = 0, \quad k = 0, 1, \dots, N_\omega^{(A)} - 1, \quad (24)$$

where y_k denotes the collocation points in the physical subdomains. We have calculated these collocation points from the Chebyshev-Gauss points $x_k^{(A)}$

$$x_k^{(A)} = \cos\left(\frac{(2k+1)\pi}{2N^{(A)}}\right), \quad k = 0, 1, \dots, N^{(A)} - 1, \quad (25)$$

and from the maps (13) and (14). Here $N^{(A)}$ denotes either $N_\psi^{(A)}$ or $N_\omega^{(A)}$.

We have approximated the field equations into a set of ordinary differential equations written in the following matricial form

$$\mathbf{M} \begin{pmatrix} \partial\bar{\psi}_k^{(1)} \\ \partial\bar{\psi}_k^{(2)} \\ \partial\bar{\omega}_j^{(1)} \\ \partial\bar{\omega}_j^{(2)} \end{pmatrix} = \mathbf{B}, \quad (26)$$

for all $k = 0, 1, \dots, N_\psi^{(A)} - 1$ and $j = 0, 1, \dots, N_\omega^{(A)} - 1$. In the above expression we have

$$\partial\bar{\psi}_k^{(A)}(u) \equiv \left(\frac{\partial\bar{\psi}^{(A)}}{\partial u}\right)_k = \sum_{i=0}^{N_\psi} a_{i,u}^{(A)}(u) \Psi_i^{(A)}(y_k), \quad (27)$$

$$\partial\bar{\omega}_j^{(A)}(u) \equiv \left(\frac{\partial\bar{\omega}^{(A)}}{\partial u}\right)_j = \sum_{i=0}^{N_\omega} b_{i,u}^{(A)}(u) \Phi_i^{(A)}(y_k), \quad (28)$$

where $\partial\bar{\psi}_k^{(A)}(u)$ and $\partial\bar{\omega}_j^{(A)}(u)$ are the values of the derivatives of $\bar{\psi}^{(A)}$ and $\bar{\omega}^{(A)}$ with respect to u at the collocation points. Note that these values are related to the time derivatives of the unknown modes $a_{k,u}^{(A)}(u), b_{j,u}^{(A)}(u)$. The matrices \mathbf{M} and \mathbf{B} depend on the unknown modes $a_k^{(A)}(u), b_j^{(A)}(u)$ as well the values of $\bar{\psi}^{(A)}$ at the collocation points, or

$$\bar{\psi}_k^{(A)}(u) \equiv \bar{\psi}^{(A)}(u, y_k) = \sum_{i=0}^{N_\psi} a_i^{(A)}(u) \Psi_i^{(A)}(y_k), \quad (29)$$

that provides a set of relations between the values and the unknown modes. The integration is performed as follows: starting from the initial modes $a_k^{(A)}(u_0), b_k^{(A)}(u_0)$ we can determine the initial values $\bar{\psi}_k^{(A)}(u_0)$ as well the initial matrices \mathbf{M}, \mathbf{B} . The dynamical system gives the initial values $\partial\bar{\psi}_k^{(A)}(u_0), \partial\bar{\omega}_j^{(A)}(u_0)$ that allows to determine $a_{k,u}^{(A)}(u_0), b_{k,u}^{(A)}(u_0)$, and as a consequence, the modes at the next time step repeating the whole process. We have used a fourth-order Runge-Kutta integrator in all cases.

4. Numerics

We compare the domain decomposition algorithm with the single domain one [24] by reproducing numerically some exact initial profiles of the gravitational potentials. In the first example, we have considered the exact Weber-Wheeler [27] solution that corresponds to the case $\omega = 0$. The exact solution $\psi_{\text{exact}} = \psi_{\text{exact}}(u, y)$ shown in the Appendix B has two parameters, A_0 and a identified as the amplitude and the width of the wave, respectively. We have set $A_0 = 1$, $a = 2$ and $u_0 = -10$ to characterize an initial profile with a step slope. The corresponding numerical profiles derived using the single domain algorithm [24] with $N_\psi = 60$ and the domain decomposition algorithm taking the truncation orders $N_\psi^{(1)} = N_\psi^{(2)} = 20$ are shown in Fig. 2. It is evident the effectiveness of the domain decomposition in reproducing the initial profile with a smaller global truncation order.

The second example is the initial profiles of both gravitational potentials from the Xanthopoulos exact solution [25] (Appendix B) where we assumed $u_0 = -10$ to produce profiles with steep slopes. Fig. 3 shows qualitatively the efficiency of the domain decomposition scheme (truncation orders $N_\psi^{(A)} = 20$, $N_\omega^{(A)} = 20$, $A = 1, 2$) over the single domain procedure ($N_\psi = N_\omega = 60$).

Using the Bondi formula presented by Stachel [21] we made the basic convergence test for the evolved cylindrical gravitational waves. For the sake of completeness the referred formula of Bondi is

$$\frac{dM}{du} = - \left[\left(\frac{dc_1}{du} \right)^2 + \left(\frac{dc_2}{du} \right)^2 \right], \quad (30)$$

where $M(u)$ is the Bondi mass aspect (indeed mass per unit of length), dc_1/du and dc_2/du are the news functions associated to each degree of freedom of the gravitational waves. These quantities are calculated according to

$$M(u) = \frac{1}{2} \lim_{y \rightarrow \infty} \gamma, \quad (31)$$

$$\frac{dc_1}{du} \equiv \lim_{y \rightarrow \infty} \bar{\psi}_{,u}, \quad (32)$$

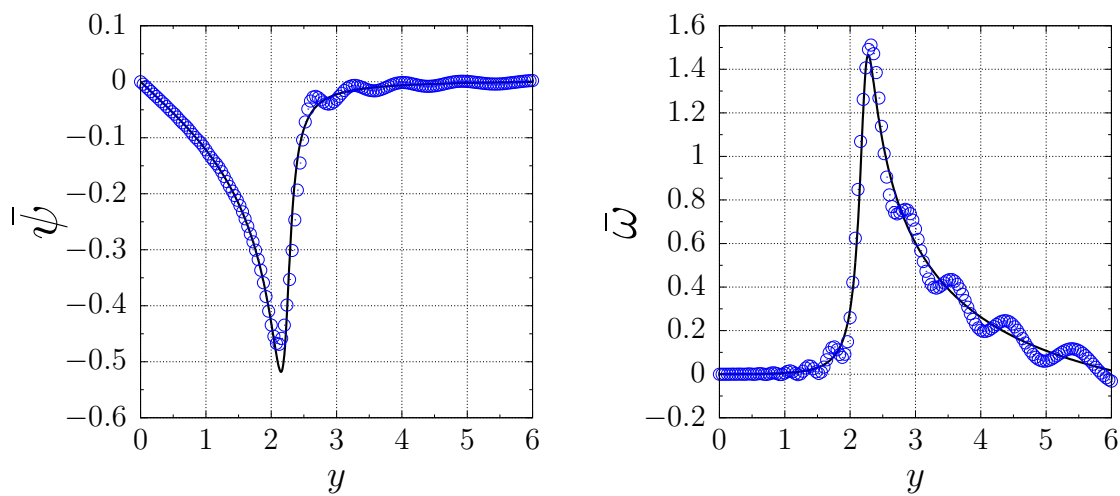
$$\frac{dc_2}{du} \equiv \frac{1}{2} \lim_{y \rightarrow \infty} \left(e^{2\bar{\psi}/y} \bar{\omega} \right)_{,u}. \quad (33)$$

To measure a deviation from the Bondi formula due to the numerical solution, we introduced the function $C(u)$ defined by

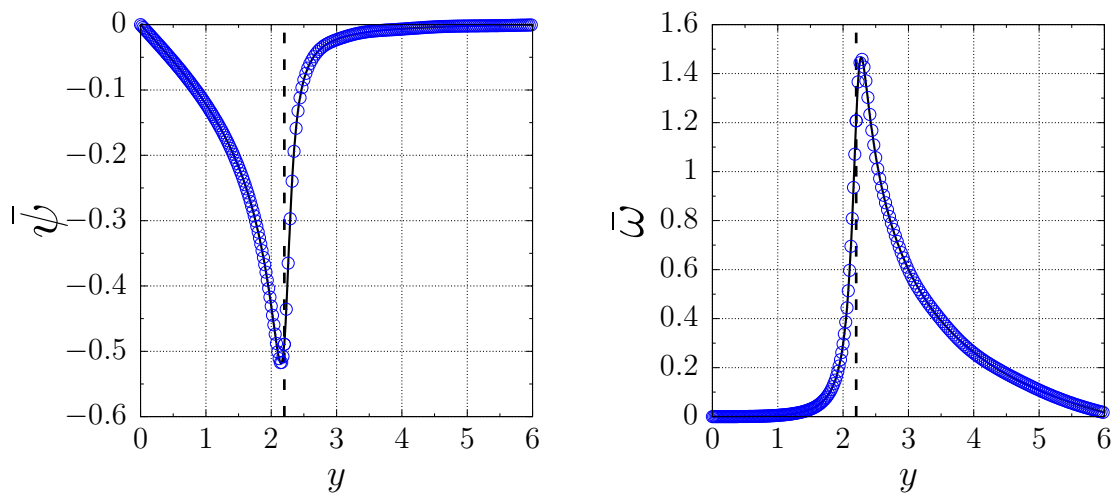
$$C(u) = \left| \frac{1}{2\delta u} (M(u + \delta u) - M(u - \delta u)) + \left(\frac{dc_1}{du} \right)^2 + \left(\frac{dc_2}{du} \right)^2 \right|, \quad (34)$$

where we approximate the derivative of the Bondi mass using the central difference scheme.

The last numerical test consisted in determining the maximum value of $C(u)$ in function of $N = N^{(1)} + N^{(2)}$, where $N^{(A)}$, $A = 1, 2$ denote the truncation orders in each subdomain.



(a)



(b)

Figure 3. Initial exact profile provided by the Xanthopoulos’ solution. We have set $u_0 = -10$, $L_0 = 3$ and we have placed the interface at $y_0 = 2.3$. As before the circles indicate the numerical solution and the continuous lines the exact solution. In (a) and (b) we have generated the results using the single and the domain decomposition algorithms, respectively.

We evolved the cylindrical waves with the initial configurations shown in Figs. 2 and 3 corresponding to the initial profiles of the Weber-Wheeler and the Xanthopoulos solutions for $u_0 = -10$, respectively. The results are presented in Fig. 5 with the exponential decay of the maximum deviation of the Bondi formula, C_{\max} .

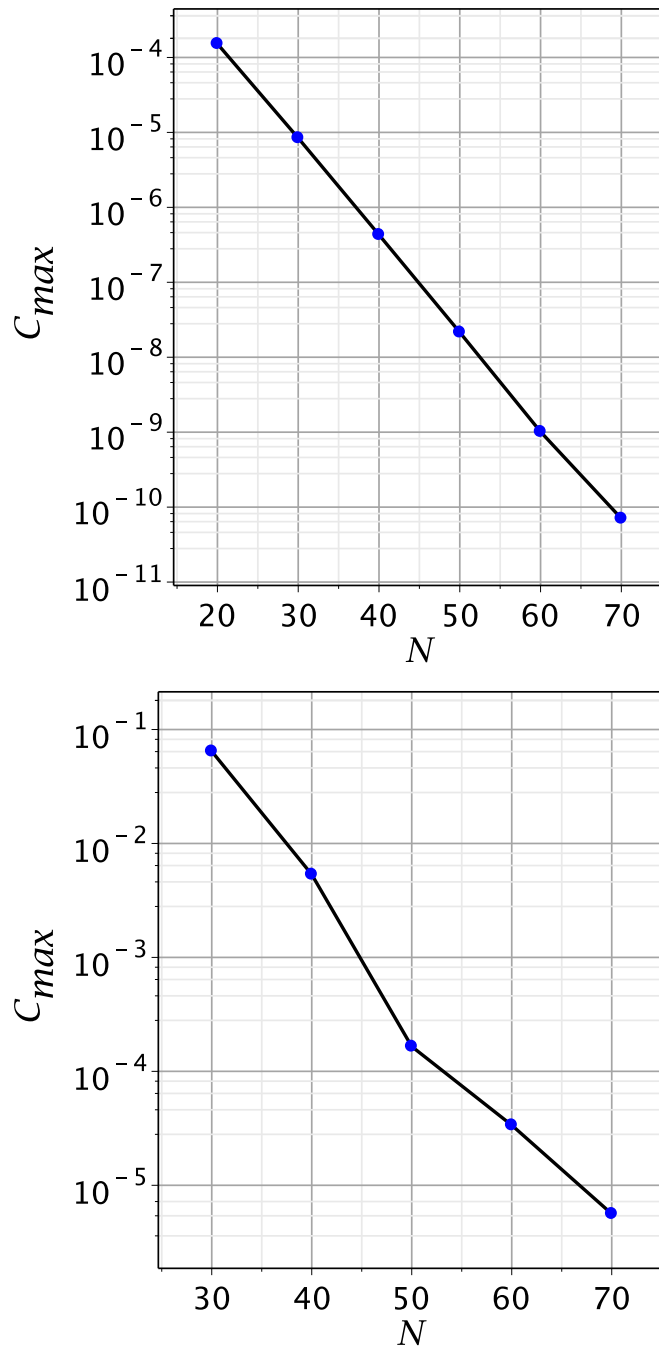


Figure 4. Exponential decay of the maximum deviation of the Bondi formula, C_{max} (cf. Eq. (34)), in function of the truncation order in each domain, $N = N_{\psi}^{(A)} = N_{\omega}^{(A)}$, $A = 1, 2$. In the upper panel, we evolved the spacetime with the initial data shown in Fig. 2. In the lower panel, the initial data is provided by the exact Xanthopoulos solution shown in Fig. 3. We found that $y_0 = L_0 = 2.1$ produced the best convergence

5. Templates of the gravitational waves

The peeling theorem plays a crucial role in characterizing the gravitational radiation emitted by an isolated source. After the works of Sachs [28] and Newman and Penrose [29], all the information containing in the Weyl tensor is expressed by five complex scalars known as the Weyl scalars. We denote these quantities by Ψ_n , $n = 0, 1, \dots, 4$, obtained after a convenient projection of the Weyl tensor in a null complex tetrad basis.

We can summarize the peeling theorem by the following behaviors of the Weyl scalars in a neighborhood of the future null infinity \mathcal{J}^+ :

$$\Psi_n \sim \frac{1}{r^{5-n}}, \quad (35)$$

where r is the affine parameter along the null rays. In particular, the Weyl scalar Ψ_4 falls off as r^{-1} indicating that the gravitational field behaves like a plane wave asymptotically. Therefore, if distinct from zero, Ψ_4 provides a measure of the outgoing gravitational wave at the radiation zone, or at a large distance from the source. As a consequence, we can express the Peeling theorem [28] in terms of the Weyl tensor projected with respect to the null tetrad basis such that

$$C_{abcd} = \frac{N_{abcd}}{r} + \frac{III_{abcd}}{r^2} + \frac{II_{abcd}}{r^3} + \frac{I_{abcd}}{r^4} + \dots, \quad (36)$$

where $N_{abcd}, III_{abcd}, \dots$ denote tensors with the algebraic structure of the Riemann tensors of Petrov types N, III, \dots , respectively. Those spacetimes of type N contain gravitational radiation whose templates associated to each polarization mode are given by the real and imaginary parts of N_{abcd} or

$$N_{abcd} \equiv (r\Psi_4)_\infty = \lim_{r \rightarrow \infty} r\Psi_4. \quad (37)$$

Stachel [21] exhibited a version of the peeling theorem for the general cylindrical spacetimes, but the asymptotic expansion of the Riemann tensor is with inverse integer powers of $\rho^{\frac{1}{2}}$ since the spacetime is not asymptotically flat. It means that the Weyl scalars fall off as

$$\Psi_n \sim \frac{1}{y^{5-n}}. \quad (38)$$

Hence, for cylindrical spacetimes the Weyl scalar Ψ_4 describes the outgoing gravitational radiation at the wave zone. By choosing a convenient null tetrad basis shown in the Appendix C, the following real and imaginary parts provides the template of the waves at the wave zone corresponding to the mode $+$ and \times , respectively

$$(y\Psi_4)_\infty = \lim_{y \rightarrow \infty} e^{-2\gamma}(2\bar{\psi}_{,u}\gamma_{,u} - \bar{\psi}_{,uu}) + i \lim_{y \rightarrow \infty} \frac{1}{2}e^{-2\gamma}(-2\bar{\omega}_{,u}\gamma_{,u} + \bar{\omega}_{,uu}). \quad (39)$$

In this Section, we extract the numerical wave templates for some cases of interest after substituting the approximations given by Eqs. (15) and (16) ($A = 2$) into Eq. (39). The asymptotic expressions for $\gamma_{,u}(u, y)$ and $\gamma(u, y)$ are calculated from Eqs. (7), (8) and (31),

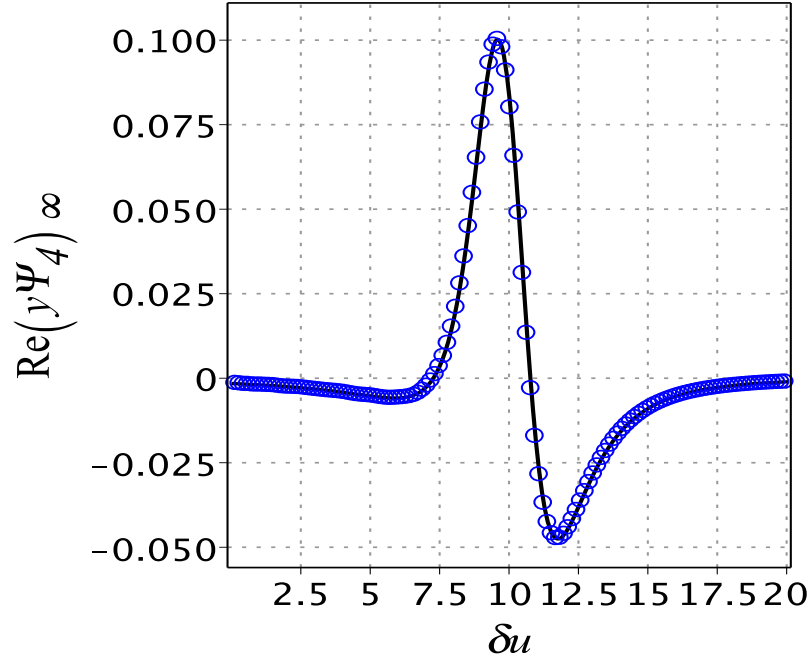


Figure 5. Exact (continuous line) and numerical (circles) templates of the Weber-Wheeler solution. The initial configuration is the same of Fig. 2, and we have set $N_\psi^{(1)} = N_\psi^{(2)} = 40$, and map parameter $L_0 = 2.0$. Here $\delta u = u - u_0$, with $u_0 = -10$.

respectively. The approximate $(y\Psi_4)_\infty$ is related to the modes $a_k^{(2)}, b_k^{(2)}$ whose evolution is dictated by the dynamical system given by Eq. (25) after setting the initial configuration.

The first case is the exact Weber-Wheeler solution describing a polarized gravitational wave that hits the symmetry axis to rebound back to infinity. The real part of Eq. (39) determines the template at the radiation zone. Starting with the initial profile of Fig. 2, we present in Fig. 5 the exact (line) and the numerical (circles) plots of $\text{Re}(y\Psi_4)_\infty$. The excellent agreement between the exact and numerical wave templates is another illustration of the superior accuracy of the domain decomposition algorithm (we chose truncation orders $N_\psi^{(1)} = N_\psi^{(2)} = 40$). We proceed by evolving polarized gravitational waves starting with other initial data families

$$\bar{\psi}_0(y) = A_0 y e^{-(y-y_1)^2/\sigma^2}, \quad (40)$$

$$\bar{\psi}_0(y) = A_0 y^2 \left[1 - \tanh \left(\frac{(y-y_2)^2}{\sigma^2} \right) \right], \quad (41)$$

where we fixed $\sigma = 0.5$ and $y_1 = y_2 = 3.0$. Although distinct in details, the profiles displayed in Fig. 6 have similar structure since both represent a polarized wave + that hits the axis and rebound.

In the next example, we obtain the templates resulting from the nonlinear interaction between the gravitational waves with polarization + and \times . We choose an initial data that

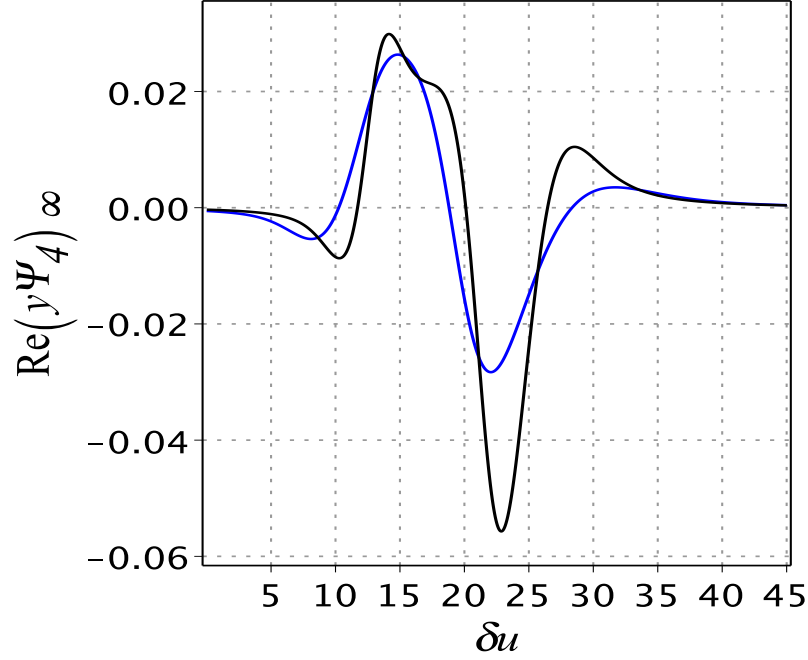


Figure 6. The wave templates for the Einstein-Rosen waves generated by the initial data families (39a) (blue) and (39b) (black) shown by the upper and lower panels, respectively. We have set $y_1 = y_2 = 3.0$, $\sigma = 0.5$ and the map parameter $L_0 = 2.5$.

contains a pure ingoing wave with polarization \times . It means that $\bar{\psi}(u_0, y) = 0$, and

$$\bar{\omega}(u_0, y) = \frac{B_0}{y} F(y^2), \quad (42)$$

where B_0 denotes the wave amplitude and F is an arbitrary function. The above expression arises after imposing that the outgoing wave \times described by the quantity O_\times [17] vanishes initially:

$$O_\times = \frac{e^{\frac{2\bar{\psi}}{y}}}{y^2} \left(2y\bar{\omega}_{,y} - \frac{(y\bar{\omega})_{,y}}{2y} \right) = 0. \quad (43)$$

The general solution is $B_0 F(y^2 + (u - u_0)/2)/y$, where the arbitrary function F satisfies the boundary conditions for $\bar{\omega}$ (see Eqs. (10) and (12)). A convenient choice for F is

$$F(y^2) = \frac{y^4}{(1 + y^4)} e^{-(y^2 - \alpha_0^2)^2 / \sigma^2}, \quad (44)$$

where α_0 and σ are parameters.

When an initially ingoing gravitational wave with polarization \times (I_\times) is directed towards the symmetry axes, the nonlinear interaction between both waves modes enters into action producing the ingoing and outgoing wave modes $+$ (I_+, O_+), along with an outgoing wave mode \times (O_\times). Therefore, the result is an unpolarized gravitational wave exhibiting templates described by $\text{Re}(y\Psi_4)_\infty(u)$ and $\text{Im}(y\Psi_4)_\infty(u)$. Moreover, Piran, Safier and Stark showed

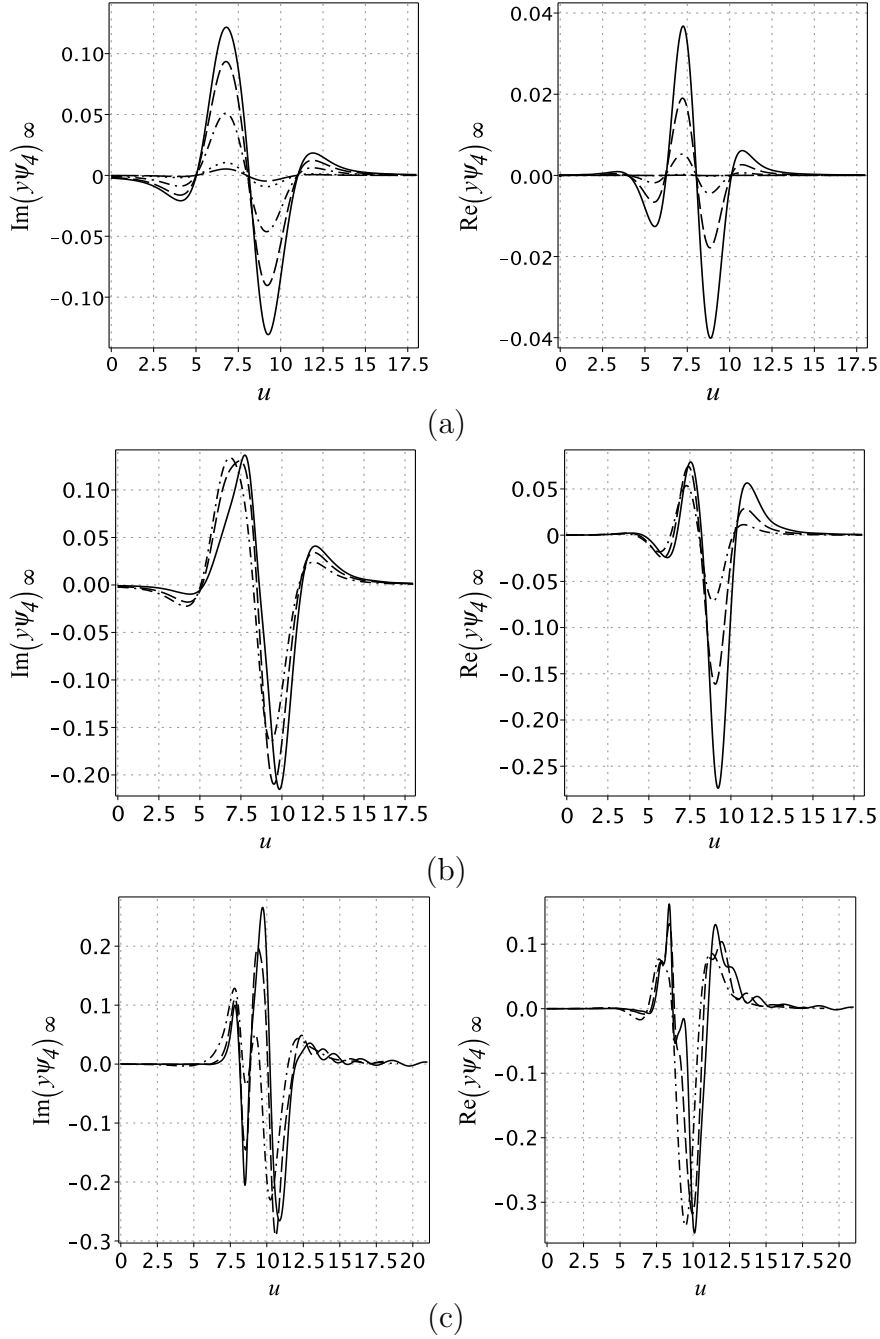


Figure 7. (a) Wave templates for the modes \times (left) and $+$ (right) for $B_0 = 0.05, 0.1, 0.5, 1.0, 1.0, 1.5$ represented by long dash, dot, dash dot, dash and solid lines, respectively. (b) Wave templates for $B_0 = 2.0, 3.0, 4.0$ represented by dash dot, dash and solid lines, respectively. (c) Wave templates for $B_0 = 5.0, 6.0, 6.5$ represented by dash dot, dash and solid lines, respectively.

an additional consequence of the interaction of both modes characterized by the rotation between I_+ and I_\times , O_+ and O_\times , or in the analog of the Faraday effect of electrodynamics. It is, therefore, a valuable task to generate the wave templates in the present context.

We evolved the spacetime starting with the initial data (40), (42) setting $\alpha_0 = 2$, $\sigma = 1.0$ and increasing values of the amplitude B_0 . We display in Fig. 7(a) the templates generated after choosing $B_0 = 0.05, 0.1, 0.5, 1.0$ and 1.5 . The patterns associated with the wave modes \times and $+$ oscillate with a phase shift as a consequence of the gravitational Faraday effect [17]. For $B_0 = 0.05$ and 0.1 the average amplitudes of $\text{Re}(y\Psi_4)_\infty$ are about 10^{-5} and 10^{-4} , respectively, therefore both signals are indistinguishable in the plot.

Increasing further B_0 the nonlinear coupling between the wave modes \times and $+$ turn to be more effective. With $B_0 = 2.0, 3.0, 4.0$ shown in Fig. 7(b), we notice that the average amplitude of the signal $\text{Im}(y\Psi_4)_\infty$ almost does not change, while there is considerable growth in the average amplitude of $\text{Re}(y\Psi_4)_\infty$. It is noteworthy the accentuated growth in the amplitude of the mode $+$ from about 10^{-5} for $B_0 = 0.05$ to 10^{-1} for $B_0 = 4.0$. In Fig. 7(c) the amplitudes are $B_0 = 5.0, 6.0, 6.5$. As noticed there is a change in the pattern structure of both wave modes with more oscillations and the appearance of tails as a consequence of the strong reflection of the ingoing radiation and the rapid production of the ingoing and outgoing wave modes $+$.

6. Final remarks

We developed a version of the Galerkin-Collocation method with the technique of domain decomposition to evolve general cylindrical gravitational waves. The advantage of the domain decomposition over the single domain code becomes evident when the potentials $\bar{\psi}(u, y)$ and $\bar{\omega}(u, y)$ have high gradients in some regions of the spatial domain.

We would like to highlight two relevant aspects. The first is the way we have introduced the computational domains schematically illustrated in Fig. 1 and described more precisely by the maps (13) and (14) that cover the whole spatial domain. The second aspect is, in general, the basis functions have a simple form if compared with those used in the single domain code (cf. Ref. [24]).

The numerical tests show the effectiveness of the domain decomposition algorithm. The first was to compare the approximate numerical initial data obtained in the single and double domains algorithms with the exact solutions of Weber-Wheeler and Xanthopoulos, where the initial data extracted from these solutions presented a region of steep variation. The second test was to evolve these data corresponding to polarized and non-polarized gravitational waves and keep track of the maximum deviation of the Bondi formula (33). By increasing the number of grid points in each domain, the error decays exponentially as expected.

In the sequence, we exhibited the templates of cylindrical gravitational waves described by the Weyl scalar Ψ_4 , with real and imaginary components corresponding to the wave modes of polarization $+$ and \times . The simplest case is of a polarized Einstein-Rosen wave (polarization $+$) that hits the axis and rebound. The corresponding template has a basic structure not changed considerably by the initial data. The most interesting case is a pure ingoing wave with polarization \times that, due to the nonlinearities entering into action, produces the ingoing and outgoing wave mode $+$. By increasing the initial amplitude of the ingoing

wave mode \times (parameter B_0) we noticed three main aspects. The wave templates $+$ and \times oscillate with a phase shift possibly as a consequence of the gravitational Faraday effect. The second aspect is a rapid growth of the wave mode $+$ if compared with the growth in the amplitude of the template \times when we increase B_0 . And finally, both wave templates display a richer structure for a high amplitude initial incoming wave with polarization \times which signalizes the strong field effect.

Acknowledgments

The authors acknowledge the financial support of the Brazilian agencies Conselho Nacional de Desenvolvimento Científico e Tecnológico (CNPq) and Coordenação de Aperfeiçoamento de Pessoal de Nível Superior (CAPES). H. P. O. and W. O. B. thank Fundação Carlos Chagas Filho de Amparo à Pesquisa do Estado do Rio de Janeiro (FAPERJ) for support within the Grant No. E-26/202.998/518 2016 Bolsas de Bancada de Projetos (BBP), and Bolsa de Pesquisador, respectively.

Appendix A. Basis functions

First we define the auxiliary basis $\chi_k(y)$ as

$$\chi_k(y) = \frac{1}{2}TL_{k+2}^{(1)}(y) + \frac{k+1}{2k+1}TL_{k+1}^{(1)}(y) + \frac{2k+3}{4(2k+1)}TL_k^{(1)}(y) \quad (\text{A.1})$$

and the basis functions $\Phi_k^{(1)}(y)$ are

$$\Phi_k^{(1)}(y) = \frac{1}{4}\chi_k(y) + \frac{(2k^2 + 5k + 3)}{4(2k^2 + 9k + 9)}\chi_{k+1}(y). \quad (\text{A.2})$$

Appendix B. Exact solutions: the Weber-Wheeler and the Xanthopoulos solutions

The particular Weber-Wheeler solution is given by [27]

$$\psi_{\text{exact}}(u, y) = A_0 \left\{ \frac{\{a^2 + y^4 + (u + y^2)^2 [2a^2 - 2y^4 + (u + y^2)^2]\}^{1/2} + a^2 - u^2 - 2uy^2}{a^2 + y^4 + (u + y^2)^2 [2a^2 - 2y^4 + (u + y^2)^2]} \right\}^{1/2}, \quad (\text{B.1})$$

where A_0 and a are parameters identified as the amplitude and the width of the wave, respectively.

From Ref. [25] and after a straightforward calculation, the exact expressions for the potentials $\bar{\psi}$ and $\bar{\omega}$ in null coordinates $u, \rho = y^2$ are

$$\bar{\psi}_{\text{exact}}(u, y) = \frac{y}{2} \log \left[\frac{p^2(\eta^2 + \mu^2) + \mu^2 + 1}{(1 - p\eta)^2 + (1 + p^2)\mu^2} \right], \quad (\text{B.2})$$

$$\bar{\omega}_{\text{exact}}(u, y) = \frac{2\sqrt{1 + p^2}(\mu^2 - 1)(1 - p\eta)}{py [p^2(\eta^2 + \mu^2) + \mu^2 - 1]}, \quad (\text{B.3})$$

where p is a free parameter, μ and η are functions of (u, y)

$$\begin{aligned} \mu(u, y) &= \frac{\Delta}{\sqrt{2}}, \\ \eta(u, y) &= \frac{\sqrt{2}(u + y^2)}{\Delta}, \end{aligned} \quad (\text{B.4})$$

and

$$\Delta = \left[-u^2 - 2uy^2 + 1 + \sqrt{(-u^2 - 2uy^2 + 1)^2 + 4(u + y^2)^2} \right]^{1/2}. \quad (\text{B.5})$$

The second parameter, α , appears in the expression of $\gamma(u, y)$ as

$$e^{2\gamma} = \frac{\alpha^2 [p^2(\eta^2 + \mu^2) + \mu^2 - 1]}{\eta^2 + \mu^2}. \quad (\text{B.6})$$

Appendix C. The null tetrad basis

We can express components of the metric tensor with respect to a set of null tetrads as

$$g_{\mu\nu} = -l_\mu k_\nu - k_\mu l_\nu + m_\mu \bar{m}_\nu + \bar{m}_\mu m_\nu, \quad (\text{C.1})$$

where l_μ, k_μ and m_μ are null vectors that satisfy the relations $l_\mu k^\mu = -m_\mu \bar{m}^\mu = -1$. After a straightforward calculation we have

$$l_\mu = e^{2(\gamma - \psi)} \delta_\mu^0, \quad (\text{C.2})$$

$$k_\mu = \frac{1}{2} \delta_\mu^0 + \delta_\mu^1 = \left(\frac{1}{2}, 1, 0, 0 \right), \quad (\text{C.3})$$

$$m_\mu = \frac{1}{\sqrt{2}} \left(0, 0, e^\psi, \omega e^\psi - i\rho e^{-\psi} \right), \quad (\text{C.4})$$

$$\bar{m}_\mu = \frac{1}{\sqrt{2}} \left(0, 0, e^\psi, \omega e^\psi + i\rho e^{-\psi} \right). \quad (\text{C.5})$$

The Newman-Penrose scalar Ψ_4 is given by

$$\Psi_4 = R_{\mu\nu\alpha\beta}\bar{m}^\mu k^\nu \bar{m}^\alpha k^\beta, \quad (\text{C.6})$$

and the corresponding real and imaginary parts are respectively

$$\begin{aligned} (\Psi_4)^{\text{real}} = & e^{2(\psi-\gamma)} \left[\frac{1}{2y} \left(\frac{\bar{\psi},u}{y} \right)_{,y} - \frac{\bar{\psi},uu}{y} - \frac{1}{16y^2} \left(\frac{\bar{\psi}}{y} \right)_{,yy} \right. \\ & + \frac{1}{16y^3} \left(\frac{\bar{\psi}}{y} \right)_{,y} + \left(\frac{1}{2y} \left(\frac{\bar{\psi}}{y} \right)_{,y} - 2\frac{\bar{\psi},u}{y} - \frac{1}{2y^2} \right) \times \\ & \left. \left(\frac{1}{4y}\gamma_{,y} - \gamma_{,u} \right) - \frac{1}{2} \left(\frac{1}{2y} \left(\frac{\bar{\psi}}{y} \right)_{,y} - 2\frac{\bar{\psi},u}{y} \right)^2 \right. \\ & \left. + \frac{e^{4\psi}}{2y^4} \left(\frac{1}{4y}(y\bar{\omega})_{,y} - y\bar{\omega},u \right) \right], \quad (\text{C.7}) \end{aligned}$$

$$\begin{aligned} (\Psi_4)^{\text{im}} = & \frac{1}{2y} e^{2(2\psi-\gamma)} \left[\left(\frac{1}{2y^2}(y\bar{\omega})_{,y} - \bar{\omega},u \right) \left(\frac{3}{2y} \left(\frac{\bar{\psi}}{y} \right)_{,y} - \frac{6\bar{\psi},u}{y} \right. \right. \\ & \left. \left. - \frac{\gamma_{,y}}{2y} + 2\gamma_{,u} - \frac{1}{2y^2} \right) - \frac{(y\bar{\omega},u)_{,y}}{2y^2} + \bar{\omega},uu + \frac{1}{16y^3} \times \right. \\ & \left. \left((y\bar{\omega})_{,yy} - \frac{(y\bar{\omega})_{,y}}{y} \right) \right]. \quad (\text{C.8}) \end{aligned}$$

References

- [1] Grandclément P and Novak J 2009 *Living Rev. Relativ.* **12** 1
- [2] Kidder L E and Finn L S 2000 *Phys. Rev. D* **62** 084026
- [3] Canuto C, Quarteroni A, Hussaini M Y and Zang T A 1988 *Spectral Methods in Fluid Dynamics* (Springer-Verlag)
- [4] Gottlieb D and Hesthaven J S 2001, *J. Comp. App. Math.* - Special issue on Numerical Analysis, Vol VII: Partial Differential Equations, 128, 1 - 2, 83
- [5] Gottlieb D and Orszag S A, 1977 *Numerical Analysis of Spectral Methods: Theory and Applications*, SIAM
- [6] Kopriva D A 1986 *App. Num. Math.* **2** 221
- [7] Orszag S 1980 *J. Comp. Phys.* **37** 70
- [8] Kopriva D A 1989 *SIAM J. Sci. Stat. Comput.* **10** 120
- [9] Bonazzola S, Gourgoulhon E, Salgado M and Marck J A 1993 *Astron. Astrophys.* **278** 421
- [10] Pfeiffer H P 2003 *Initial data for black hole evolutions*, Ph.D. thesis, arXiv:gr-qc/0510016
- [11] Ansorg M 2007 *Class. Quantum Grav.* **24** S1
- [12] Spectral Einstein Code, <https://www.black-holes.org/code/SpEC.html>
- [13] LORENE (Langage Objet pour la Relativité Numérique), <http://www.lorene.obspm.fr>

- [14] Kidder L E, Scheel M A and Teukolsky S A 2000 *Phys. Rev. D* **62** 084032
- [15] Szilágyi B, Lindblom L and Scheel M A 2009 *Phys. Rev. D* **80** 124010
- [16] Patera A T 1984 *J. Comp. Phys.* **54** 468
- [17] Piran T, Safier P N and Stark R F 1985 *Phys. Rev. D* **32** 3101
- [18] Kompaneets A S 1958 *Zh. Eksp. Teor. Fiz.* **34** 953 (*Sov. Phys. JETP* **7** 659)
- [19] Jordan P, Ehlers J and Kundt W 1960 *Abh. Akad. Wiss. Mainz. Math. Naturwiss.* **K1** 2
- [20] Thorne K S 1965 *Phys. Rev.* **138** 251
- [21] Stachel J J 1966 *J. Math. Phys.* **7** 1321
- [22] Gonçalves S M C V 2003 *Class. Quantum Grav.* **20** 37
- [23] Dubal M R d'Inverno R A and Clarke C J S 1995 *Phys. Rev. D* **52** 6868
- [24] Celestino J, de Oliveira H P and Rodrigues E L 2016 *Phys. Rev. D* **93** 104018
- [25] Xanthopoulos B C 1986 *Phys. Rev. D* **34** 3608
- [26] Boyd J 2001 *Chebyshev and Fourier Spectral Methods*, Dover Publications
- [27] Weber J and Wheeler J A 1957 *Rev. Mod. Phys.* **29** 509
- [28] Sachs R K 1962 *Proc. Roy. Soc. A* **265** 463; *ibid.* 1962 **270** 103
- [29] Newman E T and Penrose R 1962 *J. Math. Phys.* **3**, 566; 1963 *J. Math. Phys.* **4** 998
- [30] Einstein A and Rosen N 1937 *J. Franklin Inst.* **223**, 43